Journal of Magnetism and Magnetic Materials 469 (2019) 19–27

Contents lists available at ScienceDirect

Journal of Magnetism and Magnetic Materials

journal homepage: www.elsevier.com/locate/jmmm

Research articles

Effect of multi-axial stress on iron losses of electrical steel sheets

U. Aydin[a,*], P. Rasilo[a,b], F. Martin[a], A. Belahcen[a], L. Daniel[c], A. Haavisto[a], A. Arkkio[a]

[a] Department of Electrical Engineering and Automation, Aalto University, FI-00076 Espoo, Finland
[b] Laboratory of Electrical Engineering, Tampere University of Technology, FI-33101 Tampere, Finland
[c] GeePs—Group of electrical engineering – Paris, CentraleSupélec, UMR CNRS 8507, Univ. Paris-Sud, Université Paris-Saclay, Sorbonne Université, 3& 11 rue Joliot-Curie, Plateau de Moulon, 91192 Gif-sur-Yvette Cedex, France

ARTICLE INFO

Keywords:
Excess loss
Hysteresis loss
Magneto-mechanical
Multi-axial stress
Single sheet tester

ABSTRACT

The effect of multi-axial stress on the iron losses of a non-oriented electrical steel sheet under alternating magnetization is analyzed. Multi-axial magneto-mechanical measurements on a M400-50A grade non-oriented electrical steel sheet are performed by using a custom made single sheet tester device. The measured losses are separated into hysteresis, classical and excess loss components by using statistical loss theory, and the effect of various stress configurations on the hysteresis and the excess loss components is analyzed. By utilizing the statistical lo, an equivalent stress model and a magneto-elastic invariant based model are derived. These models can be used to predict the iron loss evolution under multi-axial stress even if only uniaxial stress dependent measurements are available. The accuracy of both models to predict the multi-axial stress dependent iron losses is found to be satisfactory when they are identified only from uniaxial stress dependent measurements. The invariant based model is shown to be slightly more accurate for the studied material.

1. Introduction

The magnetic properties of electrical steel sheets widely used in electrical machine cores are known to be highly stress dependent. During the manufacturing processes and operation of these devices multi-axial stresses are exerted on the core laminations [1–6]. The performance of the electrical machines is significantly affected by these multi-axial loadings [7–12]. Therefore, in order to be able to design more efficient devices and analyse existing ones with better accuracy, the dependency of the core losses on the multi-axial stresses should be studied comprehensively.

Previously, several studies on the interaction between the different components of the core losses in electrical steel sheets and the mechanical stress have been performed [13–17]. For instance, in [13] the effect of uniaxial stress on different loss components was studied according to the statistical loss theory of [18]. It was found that the hysteresis and excess losses increased under compression and high tensile stress, and reduced under low tensile stress. A similar study with wide range of data has been performed in [14]. In both studies it was reported that the uniaxial stress has similar effect on the hysteresis and excess loss components. On the other hand, in [15] uniaxial tension dependent core losses are separated into hysteresis, excess and non-linear loss components. It was shown that the tensile stress affected the hysteresis and non-linear loss components, whereas the effect on the excess loss component was insignificant.

The aforementioned studies rely on fitting the loss model parameters to the measured losses only under various uniaxial magneto-mechanical loadings. Although they can be accurate in describing the losses within the fitted uniaxial stress ranges, they do not describe or predict the stress dependent losses under multi-axial loadings as it occurs in electrical machines. Due to the practical difficulties of performing multi-axial magneto-mechanical experiments, only a few experimental studies on non-oriented electrical steel sheets were performed in the past to study the multi-axial stress dependency of the iron losses [19–22]. For instance in [19–21], effect of uniaxial and shear stress on magnetic properties and iron losses of non-oriented electrical steel sheets was studied. However in these studies, the experiments were performed only at single magnetizing frequency which was not enough to segregate the iron losses and study the stress effects on different loss components. In addition, they did not provide any stress dependent loss model.

Since performing multi-axial magneto-mechanical measurements is practically a difficult task, a model that can be identified from uniaxial measurements to predict the multi-axial core losses is needed. Recently, in [23] equivalent stress models to predict the core losses under bi-axial stress when only uniaxial stress dependent measurements are available are proposed. However, the proposed models were only applied and validated for bi-axial configurations. In addition, in order to separate

* Corresponding author.
E-mail address: ugur.aydin@aalto.fi (U. Aydin).

https://doi.org/10.1016/j.jmmm.2018.08.003
Received 27 April 2018; Received in revised form 10 July 2018; Accepted 2 August 2018
Available online 10 August 2018
0304-8853/

the losses, they used magneto-mechanical measurements from [22] with non-sinuoidal flux density ($\boldsymbol{B}$) in the statistical loss model by Jordan that assumes sinusoidal $\boldsymbol{B}$ [24]. This approach can cause significant errors in the loss separation [25].

In this paper, measurements under controlled sinusoidal flux density with 1 T amplitude at various frequencies and under up to ± 30 MPa multi-axial in-plane stresses performed on a M400-50A non-oriented electrical steel sheet are reported. The core losses are separated into hysteresis, classical and excess loss components using Bertotti's statistical loss model [18] and the effect of multi-axial stress on the hysteresis and excess loss components is investigated. One of the equivalent stress models from [23] is tested for predicting the effect of multi-axial stress on the iron loss components when the model is fitted merely based on uniaxial measurements. Finally, a simple model based on magneto-mechanical invariants is proposed to predict the multi-axial stress dependency of the hysteresis and excess losses by utilizing the statistical loss model.

2. Magneto-mechanical measurements

A custom-made single sheet tester device which has ability to apply arbitrary magneto-mechanical loading on steel sheets was used to perform the magneto-mechanical measurements. The measurement setup and the sample geometry that consists of six legs are shown in Fig. 1. Previously, it was shown in [26] that it is possible to obtain an arbitrary in-plane stress tensor in the measurement area using a similar six-legs sample geometry. The design of the device and the control procedures are detailed in [27] and the important aspects will be summarized here. The measurement area is $20 \times 20\ \mathrm{mm}^2$ and it is located in the central area of the sample as shown in Fig. 1(a). Mechanical stresses were applied to each leg of the sample by screw guides that were driven by servo motors. Between the servo motor and the screw guide a gearbox with ratio of 60:1 was connected to obtain high stress application precision at each leg. To avoid buckling under compressive stress, the sample was reinforced from the top and the bottom by non-magnetic plates. Oil was applied on each side of the sample to minimize the friction between sample and the reinforcing plates. The mechanical strain ε in the measurement region of the sample was measured using a 10 mm diameter rosette type strain gauge with 0°−45°−90° orientation. Afterwards, the stress was calculated using the well known plane stress formulation of the Hooke's law. In order to achieve the desired stress tensor at the measurement region, stress was calculated using simultaneously measured strain and each servo was controlled to displace accordingly. The studied stress configurations were uniaxial stress along rolling (x) and transverse (y) directions, equibiaxial stress and two cases of pure shear stress. Latter two are denoted as shear-I and shear-II for brevity. In this work, the studied stress states are expressed using the notation given by $\boldsymbol{\sigma} = [\sigma_{xx} \quad \sigma_{yy} \quad \tau_{xy}]^T$. Then the studied cases, the equibiaxial, shear-I and shear-II stress configurations are expressed in this notation as $\boldsymbol{\sigma} = [\sigma \quad \sigma \quad 0]^T$, $\boldsymbol{\sigma} = [\sigma \quad -\sigma \quad 0]^T$, $\boldsymbol{\sigma} = [0 \quad 0 \quad \tau]^T$, respectively. The magnitude of σ and τ varies from -30 MPa (compression) to 30 MPa (tension) with 10 MPa intervals.

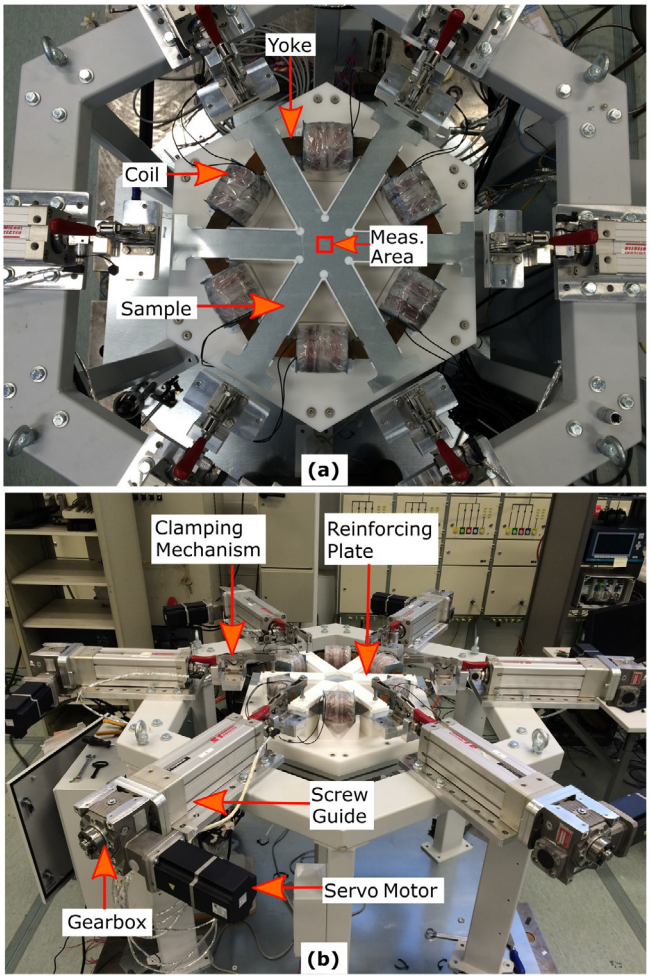

Fig. 1. Single sheet tester device shown (a) from top, (b) as a whole.

On the other hand, magnetizing coils were wound around grain-oriented laminated yokes and they were placed between each leg of the sample. The coils were supplied with controlled voltage waveform in order to obtain sinusoidal alternating flux density in the measurement area. The flux control principle is based on [28,29]. To measure magnetic flux density, two search coils of four turns each were placed at the measurement area perpendicular to each other. Magnetic field strength ($\boldsymbol{H}$) was measured using a double H-coil placed on the measurement area. The correct alignment of the H-coil was ensured by comparing clockwise and counterclockwise rotational field measurements. The measurements were performed at flux density along rolling or transverse directions with 1 T amplitude and at 10 Hz, 30 Hz, 70 Hz, 110 Hz and 150 Hz frequencies.

After the measurements of *B-H* loops, the iron loss densities (p) per period (T) are calculated for each studied case by

$$p = \frac{1}{T}\int_0^T \boldsymbol{H}\cdot\frac{\mathrm{d}\boldsymbol{B}}{\mathrm{d}t}\mathrm{d}t. \tag{1}$$

2.1. Measurements under uniaxial and biaxial stresses

The measured *B-H* loops under zero stress and uniaxial stress applied along rolling and transverse directions with $\sigma = \pm 30$ MPa where the sample is magnetized along rolling direction with 10 Hz frequency are shown in Fig. 2(a). When tension parallel to or compression perpendicular to magnetization direction are applied, the material is affected in a very similar way. At these stress conditions, the permeability of the material is improved and the coercive field is decreased slightly compared to the stress free case. On the other hand, application of compression parallel to or tension perpendicular to the magnetization direction causes reduced permeability and increased coercive field. Considering the studied uniaxial cases, the largest effect is caused by uniaxial compression along magnetization direction.

The *B-H* loops under the same magnetization conditions and under bi-axial stress are shown in Fig. 2(b). The bi-tension and shear-I configuration with tensile stress along magnetization direction improves the permeability similar to the case when uniaxial tensile stress is applied parallel to magnetization direction. The bi-compression reduces the permeability slightly, whereas shear-I case with compression along the magnetization direction reduces the permeability and increases the coercive field considerably more than the other cases.

Percentage variations of the power loss densities per cycle are

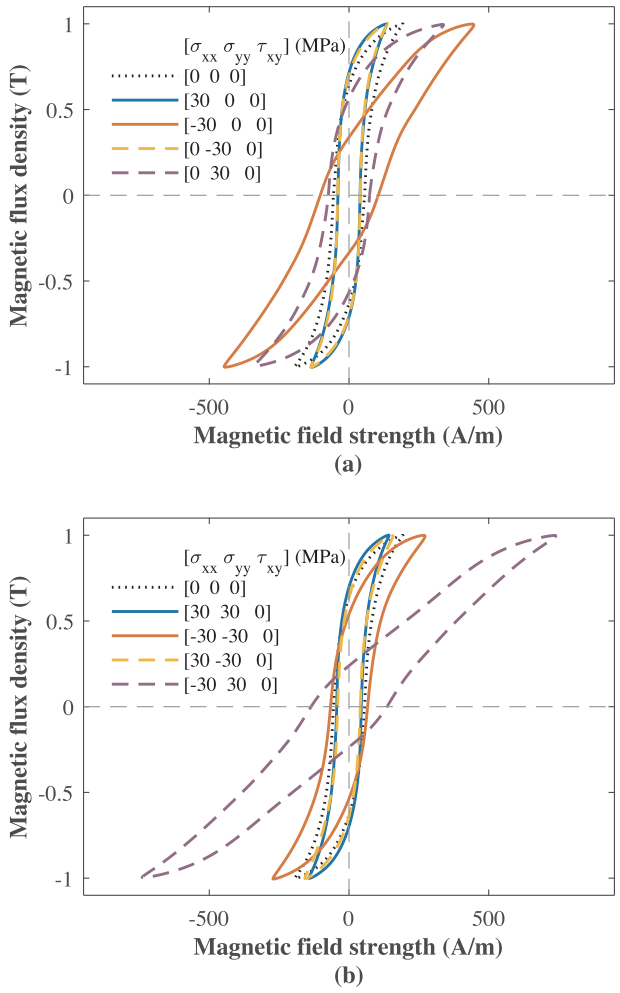

Fig. 2. Measured *B-H* loops at 1 T induction level along x direction and at 10 Hz frequency under (a) uniaxial stress, (b) bi-axial stress states where $\sigma = \pm 30$ MPa.

obtained by comparing the losses at each stress state to the stress free case by

$$\Delta p = \frac{p(\sigma_{xx}, \sigma_{yy}, \tau_{xy}) - p(0, 0, 0)}{p(0, 0, 0)} \quad (2)$$

where $p(0, 0, 0)$ and $p(\sigma_{xx}, \sigma_{yy}, \tau_{xy})$ represent the losses for the stress free and stressed cases, respectively. In the case of bi-axial loading $\tau_{xy} = 0$. In Fig. 3(a) and (b) Δp is shown for uniaxial and bi-axial cases for sample magnetized along rolling (x) direction at 10 Hz and 150 Hz frequencies, respectively. It is seen that the effect of stress on the losses at both frequencies are similar. However, at 10 Hz the variation of the losses are larger than the 150 Hz case. This is because the stress affects the different loss components in different rates, and the analysis of this will be made in detail in the next section.

It was reported in [19–21] that the stress affects the magnetic properties of the material along all the directions in the plane of the sheet. In Fig. 3 it can also be seen that the stress does not affect the material only along its application axis but also perpendicular to it. When uniaxial tensile stress is applied parallel to the magnetization direction, a decrease in the losses is observed. The losses increases with application of compression along magnetization direction. The opposite effect is observed when the uniaxial stress is applied perpendicular to the magnetization direction for both cases. Considering the biaxial stress configurations, bicompression and shear-I stress case when σ_{xx} is negative (second quadrant), increases the losses. At this magnetization state, the highest increase in the losses is observed at this shear-I case

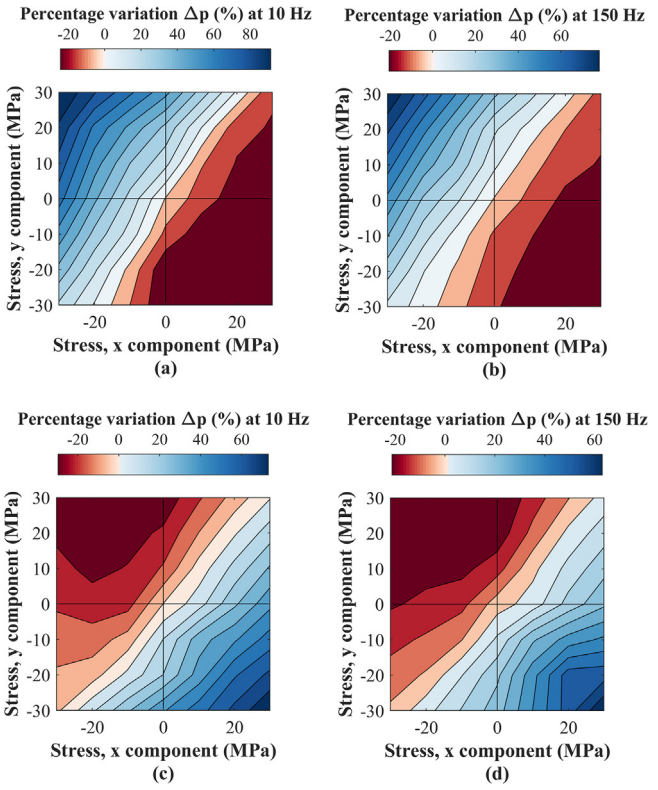

Fig. 3. Loss variations compared to the stress free case (Δp) for uniaxial and bi-axial stress states for magnetization along x direction (a) at 10 Hz frequency, (b) at 150 Hz frequency, and magnetization along y direction at (c) 10 Hz frequency, (d) 150 Hz frequency. Note the scale differences in the colormaps.

when σ_{xx} is negative. On the other hand, application of bitension and shear-I σ_{xx} being positive (fourth quadrant), decreases the losses.

In Fig. 3(c) and (d) loss evolution under same stress states when the sample is magnetized along transverse (y) direction is given. Similarly to the previous case, applied tension along magnetization direction reduces the losses, whereas compression increases it. The effect of bi-axial stress is opposite to that observed when sample is magnetized along x direction. A symmetry between Fig. 3(a), (b) and (c), (d) with respect to the $\sigma_{xx} = \sigma_{yy}$ line would be expected with an ideally isotropic material. However, the results indicate a slight difference. This behavior is associated with the magneto-elastic anisotropy of the material and it is mainly related to crystallographic texture [30]. Similar measurement results under uniaxial and multi-axial stresses were reported in [19,20,31].

2.2. Measurements under pure shear

When the shear-II stress configuration $\boldsymbol{\sigma} = [0 \;\; 0 \;\; \tau]^T$ is applied to the material, the orientation of the principal axis is not anymore aligned with the applied field. The angle of the principal stress θ_p with respect to rolling direction (x) and the principal stresses σ_1, σ_2 can be calculated by

$$\begin{aligned} \theta_p &= \tfrac{1}{2}\tan^{-1}\frac{2\tau_{xy}}{\sigma_{xx} - \sigma_{yy}} \\ \sigma_1 &= \sigma_{xx}\cos^2\theta_p + 2\tau_{xy}\cos\theta_p\sin\theta_p + \sigma_{yy}\sin^2\theta_p \\ \sigma_2 &= \sigma_{xx}\cos^2\theta_p - 2\tau_{xy}\cos\theta_p\sin\theta_p + \sigma_{yy}\sin^2\theta_p. \end{aligned} \quad (3)$$

Substituting σ_{xx}, σ_{yy} and τ_{xy} with the applied stress tensor components 0, 0, and τ yields $\theta_p = 45°$, $\sigma_1 = \tau$ and $\sigma_2 = -\tau$. An illustration of an applied shear-II stress case and the resulting principal stresses are shown in Fig. 4 for clarity. With an ideally magneto-elastically isotropic material it would be expected that the application of $\boldsymbol{\sigma} = [0 \;\; 0 \;\; \tau]^T$ and

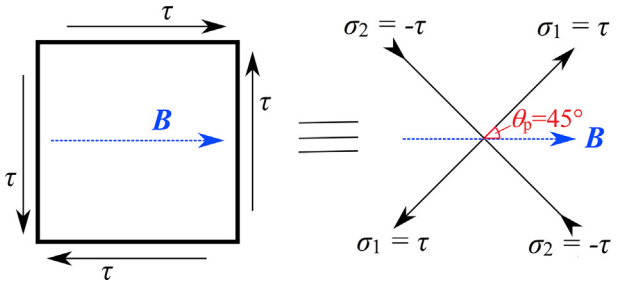

Fig. 4. Application of shear-II stress configuration and resulting principal stresses.

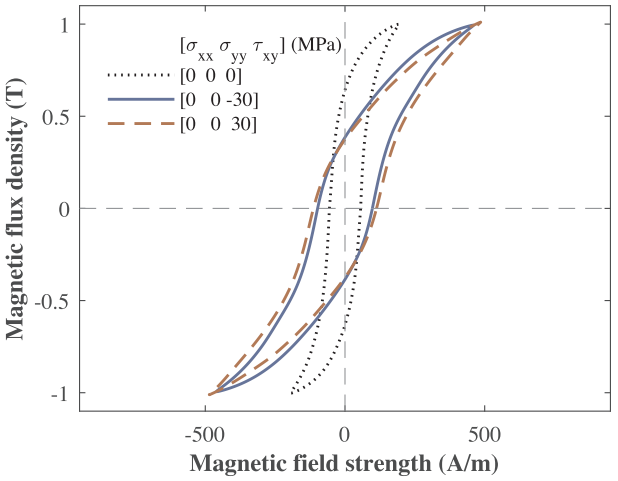

Fig. 5. Measured *B-H* loops at 1 T induction level and 10 Hz frequency under shear-II stress state where $\sigma = \pm 30$ MPa.

$\boldsymbol{\sigma} = [0 \;\; 0 \;\; -\tau]^T$ should affect the material in the same way. In Fig. 5 *B-H* loops under alternating magnetic flux density along rolling direction at 10 Hz frequency and shear-II loading with $\tau = \pm 30$ MPa is compared to the stress free case. The permeability and the coercive field is increased similarly to the case when uniaxial compression is applied along the magnetization direction. It is seen that application of $\boldsymbol{\sigma} = [0 \;\; 0 \;\; 30]^T$ and $\boldsymbol{\sigma} = [0 \;\; 0 \;\; -30]^T$ affects the material in a slightly different way since the studied material is not ideally isotropic. Similar behavior under shear stress is also reported for instance in [21].

Percentage loss variations are calculated with (2) under shear-II stress configuration where τ_{xy} varies from -30 to 30 MPa and for magnetization along x direction. The results are shown in Fig. 6(a) and (b) for 10 Hz and 150 Hz magnetization frequencies, respectively. The losses increases with similar rates under both cases when $\tau_{xy} < 0$ and $\tau_{xy} > 0$ as expected. Similarly to the bi-axial cases, under shear-II stress at 150 Hz losses increased slightly less than the case of 10 Hz. In Fig. 6(c) and (d) percentage loss variations are given for magnetization along y direction at 10 Hz and 150 Hz frequencies. The behavior is similar to the case when sample is magnetized along x direction. Similar to the bi-axial case, shear-II also affects the material at different rates depending on the magnetization direction.

3. Loss separation and proposed models

3.1. Statistical loss separation

Based on the performed magneto-mechanical measurements under sinusoidal $\boldsymbol{B}$ at 1 T fixed amplitude and at various frequencies, it is possible to separate the losses into hysteresis loss (p_{hy}), classical eddy current loss (p_{cl}) and excess loss (p_{ex}) components using the Bertotti loss model [18]. Assuming that the skin effect is negligible p_{cl} can be

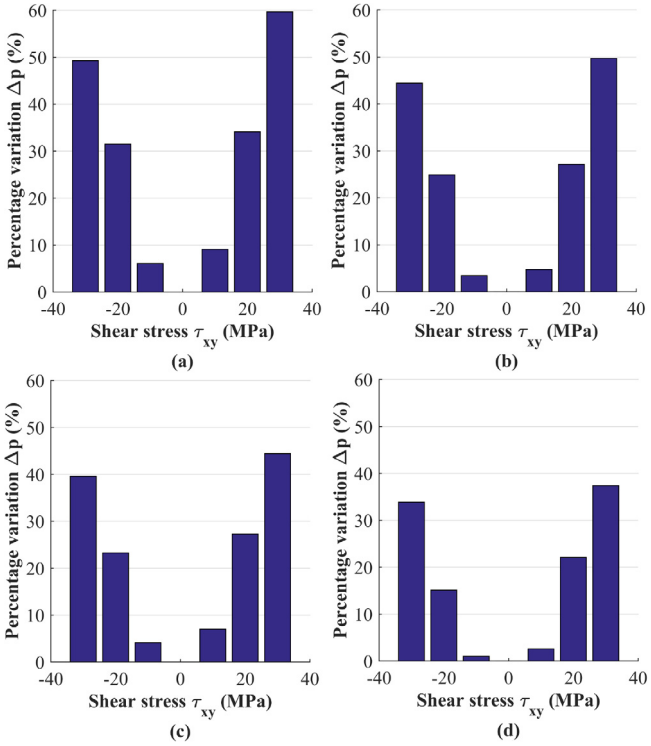

Fig. 6. Loss variations compared to the stress free case (Δp) for shear-II stress states for magnetization along x direction (a) at 10 Hz frequency, (b) at 150 Hz frequency, and magnetization along y direction at (c) 10 Hz frequency, (d) 150 Hz frequency.

determined in by

$$p_{cl} = \frac{\lambda \pi^2 d^2 B_p^2 f^2}{6} \tag{4}$$

where λ, d, B_p and f are conductivity of the material, thickness of the material, peak induction level and the frequency of the field, respectively. Then the total power loss per cycle is given for per unit volume by

$$p_{tot} = \underbrace{c_{hy} B_p^2 f}_{p_{hy}} + p_{cl} + \underbrace{c_{ex} B_p^{1.5} f^{1.5}}_{p_{ex}}. \tag{5}$$

Here, c_{hy} and c_{ex} are the hysteresis and excess loss coefficients, respectively. Since under the studied frequency levels the skin effect is negligible and the studied stress magnitudes are within the elastic limits, it is assumed that p_{cl} does not depend on the stress state of the material [13]. In order to study the effect of stress on p_{hy} and p_{ex}, the coefficients c_{hy} and c_{ex} are determined by linear least-squares fitting of (5) to the measurements for each stress state where $B_p = 1$ T applied along x or y directions and with frequencies varying from 10 Hz to 150 Hz. Considering all the cases the fitting error to the total measured losses was found to be 3.2% and 3.8% for magnetization applied along x and y directions, respectively.

The determined loss coefficients c_{hy} and c_{ex} under applied magnetization along x direction and under bi-axial stress states are shown in Fig. 7(a) and (b), respectively. In Fig. 7(c) and (d) evolution of the coefficients under the same magnetization conditions and under shear-II case is given. It is seen in Fig. 7 that the stress affects the loss coefficients c_{hy} and c_{ex} in a similar way. It is worth noting that, although the behaviors of c_{hy} and c_{ex} under stress are similar, the variation rates are different. In [13,14], similar conclusion was reported only for uniaxial stress cases.

Similarly, in Fig. 8(a) and (b) the evolution of c_{hy} and c_{ex} under biaxial stress and in Fig. 8(c) and (d) under shear-II case, where the

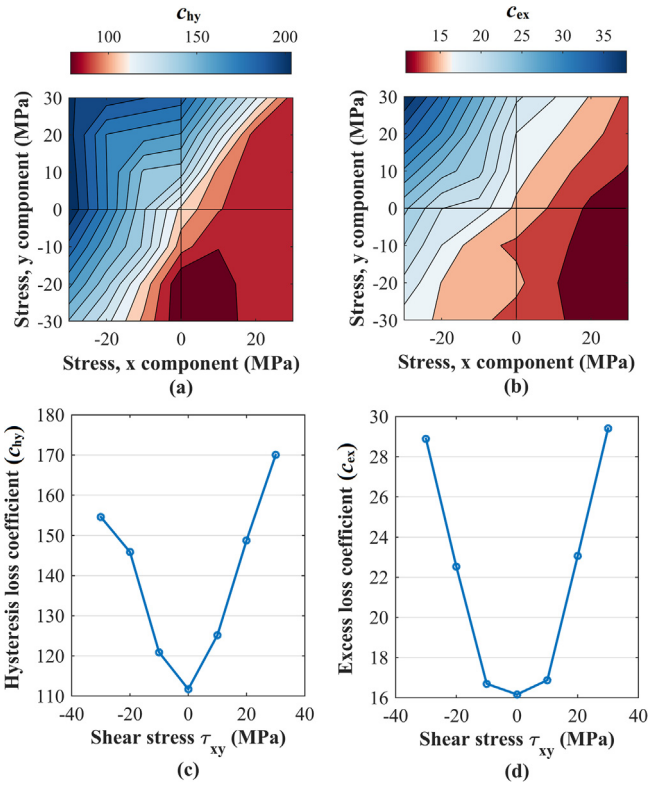

Fig. 7. For the applied magnetization along x direction, (a) evolution of c_{hy}, (b) evolution of c_{ex} under biaxial stress states and (c) evolution of c_{hy}, (d) evolution of c_{ex} under shear-II stress states.

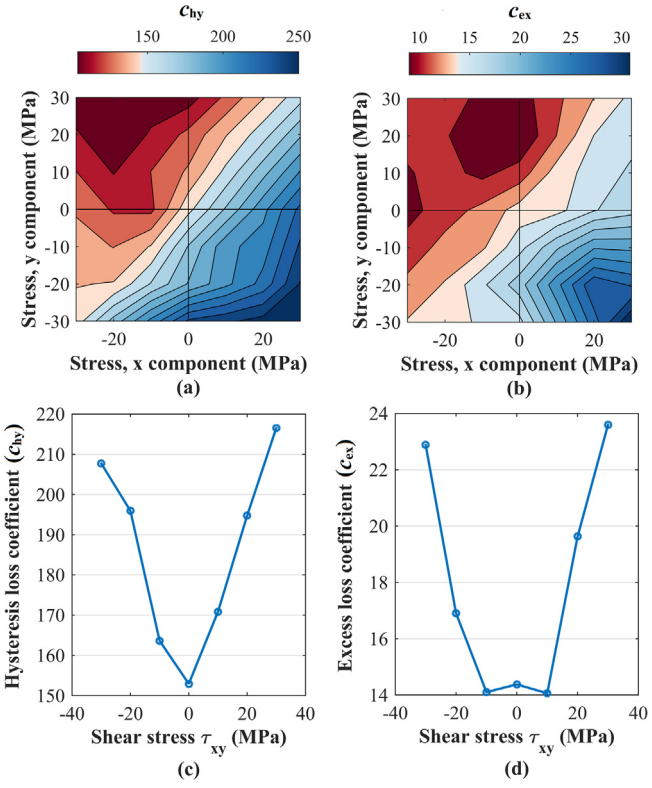

Fig. 8. For the applied magnetization along y direction, (a) evolution of c_{hy}, (b) evolution of c_{ex} under biaxial stress states and (c) evolution of c_{hy}, (d) evolution of c_{ex} under shear-II stress states.

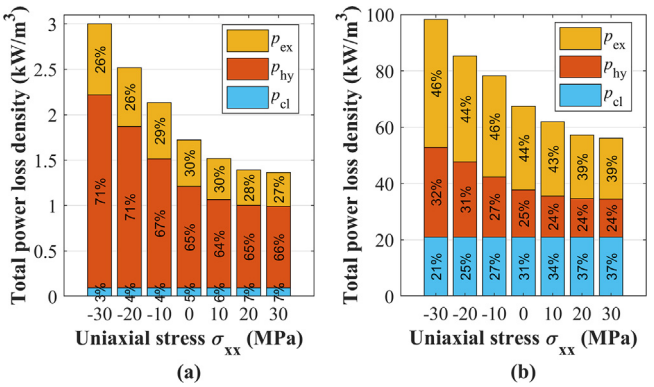

Fig. 9. Variation of different loss components for uniaxial stress applied parallel to magnetization where the sample magnetized along x direction at (a) 10 Hz, (b) 150 Hz. Rounded percentage losses of each component with respect to the total losses are also shown.

sample is magnetized along y direction is shown. Both loss coefficients are affected similarly with the stress and as in the previous case.

To analyze the effect of stress on different loss components at different frequencies in more detail, loss components under uniaxial stress applied parallel to the magnetization direction at 10 Hz and 150 Hz is shown in Fig. 9(a) and (b), respectively. The sample was magnetized along x direction. The contribution of different loss components to the total loss densities varies with frequency. At low frequency the hysteresis losses are dominant, whereas with increasing frequency the classical and the excess losses start becoming more prominent. Since c_{hy} and c_{ex} do not vary with the frequency, a change in the frequency only affects the impact magnitude of p_{hy} and p_{ex} on the total losses. That is why for instance in Figs. 3 and 6 at low frequencies the effect of stress appears to be more prominent since p_{cl} at this frequency has the least contribution which is not affected by stress.

3.2. Proposed models

A conventional way to obtain the stress free iron losses in electromagnetic devices is to use statistical iron loss models such as the Bertotti model at the post-processing stage of the simulations such as finite element analysis. This way the losses are calculated quickly and easily, since these loss models are just analytical expressions with few coefficients as described in the previous subsection. Thus, developing models to include the stress dependency to these coefficients would provide a simple and quick way to take into account the stress effects on the iron losses. In order to do that, an equivalent stress model (Model I) and a magneto-elastic invariant based model (Model II) will be studied in this subsection. In addition, their abilities to predict the multi-axial stress dependency of the iron losses will be tested.

3.2.1. Model I

The first approach adopted to model the stress dependency of the loss coefficients c_{hy} and c_{ex} is by using an equivalent stress approach (Model I). The equivalent stress approach is based on the assumption that any change caused in magnetic behavior by multi-axial stress can be modeled by an appropriate fictive uniaxial stress (equivalent stress) [32,33]. This allows predicting multi-axial magneto-mechanical behavior by utilizing the measurements under uniaxial stress only. Although the equivalent stress approach is useful, the validity of the approach is questionable and it can be inaccurate for some certain cases [34]. Nevertheless previously the equivalent stress models were used in some applications and the applicabilities of the models to take into account the stress effects were proven [8–10]. In this work, the equivalent stress definition from [23,33] is adopted and it is given by

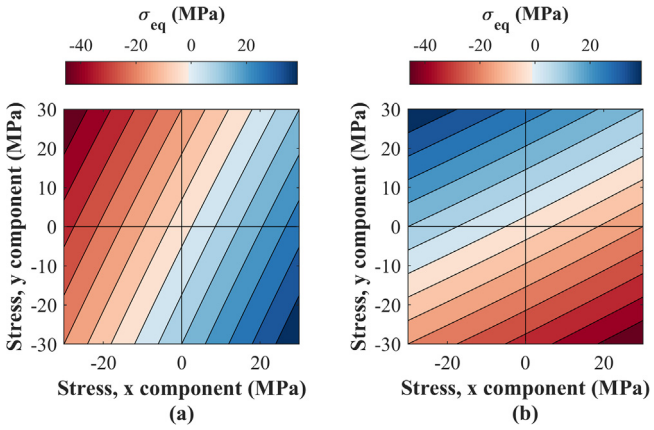

Fig. 10. Calculated equivalent stresses under biaxial stress configurations for magnetization along (a) rolling, (b) transverse directions.

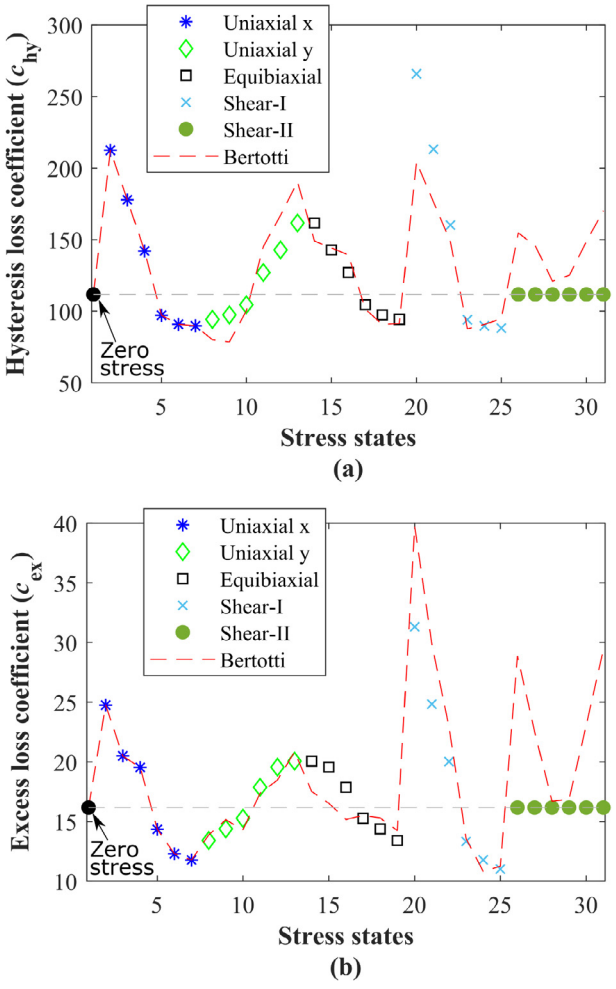

Fig. 11. Modeled loss coefficients by Model I at magnetization along x direction. (a) Hysteresis loss coefficient, (b) Excess loss coefficient. Magnitude of the applied stress varies from −30 MPa to 30 MPa with 10 MPa intervals for each stress case.

$$\sigma_{eq} = \frac{1}{K}\ln\left(\frac{2\exp(K\boldsymbol{h}^{T}\boldsymbol{s}\boldsymbol{h})}{\exp(K\boldsymbol{t}_1^{T}\boldsymbol{s}\boldsymbol{t}_1) + \exp(K\boldsymbol{t}_2^{T}\boldsymbol{s}\boldsymbol{t}_2)}\right) \quad (6)$$

where $\boldsymbol{s}$ is the deviatoric part of the applied stress tensor and it is given by $\boldsymbol{s} = \boldsymbol{\sigma} - (1/3)\mathrm{tr}(\boldsymbol{\sigma})\boldsymbol{I}$, $\boldsymbol{I}$ being the identity tensor. $\boldsymbol{h}$, $\boldsymbol{t}_1$ and $\boldsymbol{t}_2$ are the direction vectors that are parallel to applied field, orthogonal to applied field and orthogonal to the sheet plane, respectively. In (6), K is a material parameter and for silicon-iron $K = 4 \times 10^{-9}$ (m^3/J) [33]. The equivalent stresses for the studied bi-axial stress states are calculated and they are shown in Fig. 10(a) and (b) for the applied field along x and y directions, respectively. Using the previously determined Bertotti model coefficients c_{hy} and c_{ex} for the cases where uniaxial stress is applied parallel to the magnetization only, loss coefficients are modeled by the defined σ_{eq} under multi-axial stress configurations. Results are given in Fig. 11(a) and (b) for c_{hy} and c_{ex}, respectively. Coefficients under all the stress states are plotted where the magnitude of the stress varies from −30 MPa to 30 MPa with 10 MPa intervals for each configuration. The agreement under all the stress cases is satisfactory except the shear-II configuration. When the shear-II configuration $\boldsymbol{\sigma} = [0 \;\; 0 \;\; \tau]^T$ is applied $\sigma_{eq} = 0$. Therefore, under all shear-II configurations c_{hy} and c_{ex} remain constant. In addition, the model overestimates the effect of shear-I case $\boldsymbol{\sigma} = [-30 \;\; 30 \;\; 0]^T$ on the c_{hy} considerably. In Fig. 12 the same calculation results for the applied magnetization along y direction is shown. In this case the model is less accurate in equibiaxial and shear-I cases, especially for modelling c_{ex}.

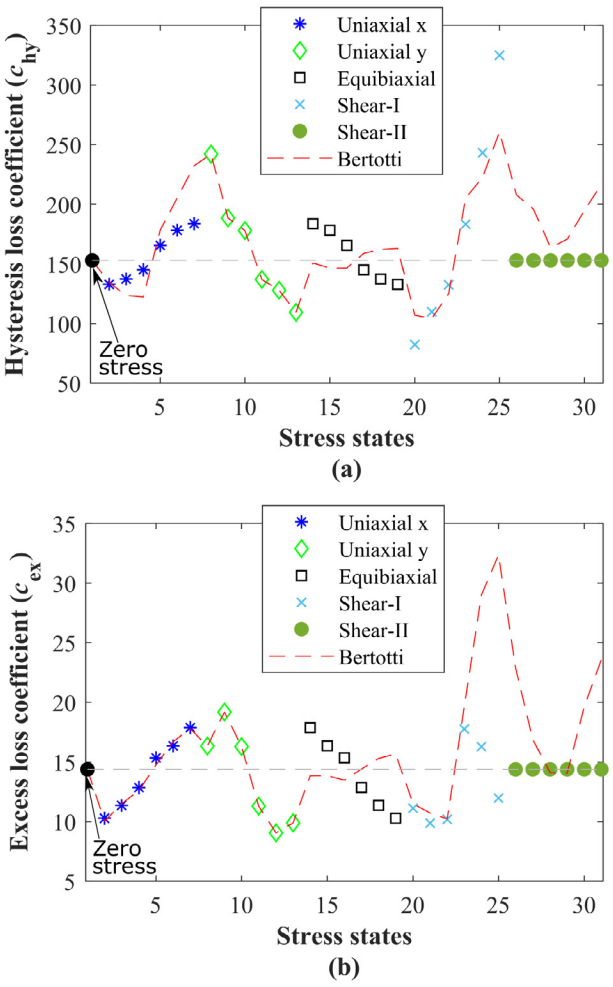

Fig. 12. Modeled loss coefficients by Model I at magnetization along y direction. (a) Hysteresis loss coefficient, (b) Excess loss coefficient. Magnitude of the applied stress varies from −30 MPa to 30 MPa with 10 MPa intervals for each stress case.

The total energy loss densities are calculated for all the stress cases and all the studied magnetization frequencies by substituting c_{hy} and c_{ex} modeled by Model I into (5) and by dividing the results with the magnetization frequency. In Fig. 13(a) and (b) the modeled results are compared to the measurements for when the magnetization is applied along x and y directions, respectively. Note that in Fig. 13 the losses are

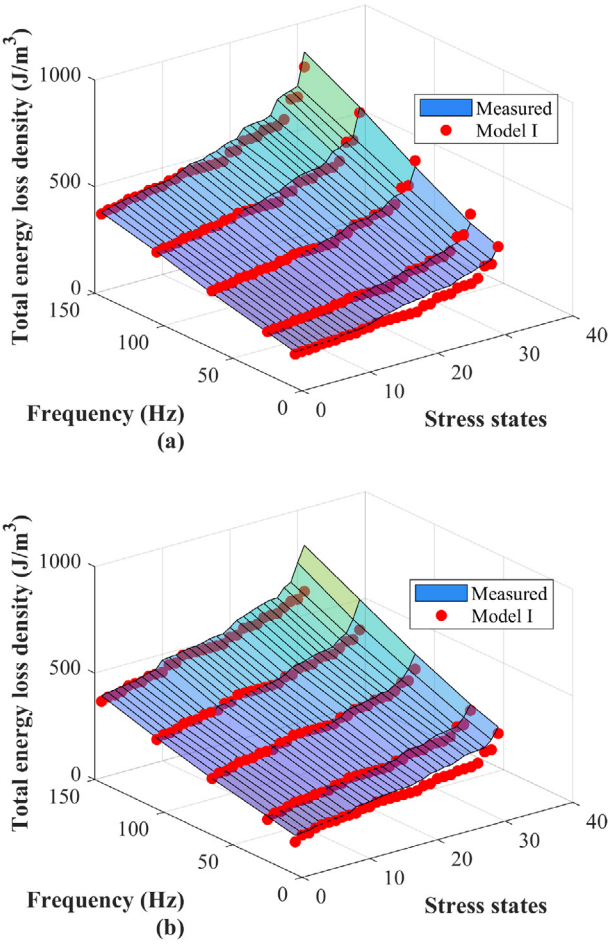

Fig. 13. Total energy loss densities for each stress and magnetization state. Measurements and modeling results from Model II (a) Magnetization along x direction, (b) Magnetization along y direction. The losses are sorted as ascending.

Table 1
Parameter values for Model II.

Parameter	Rolling direction	Transverse direction
$c_{0,\mathrm{hy}}$	115.18 (W/kg) Hz^{-1}T^{-2}	152.62 (W/kg) Hz^{-1}T^{-2}
$c_{0,\mathrm{ex}}$	16.28 (W/kg) (HzT)$^{-1.5}$	14.21 (W/kg) (HzT)$^{-1.5}$
β_h	$-2.73{\cdot}10^{-2}$MPa^{-1}	$-1.97{\cdot}10^{-2}$ MPa^{-1}
β_e	$-1.99{\cdot}10^{-2}$ MPa^{-1}	$-1.68{\cdot}10^{-2}$ MPa^{-1}
γ_h	$8.06{\cdot}10^{-4}$ MPa^{-2}	$3.51{\cdot}10^{-4}$ MPa^{-2}
γ_e	$2.68{\cdot}10^{-4}$ MPa^{-2}	$1.71{\cdot}10^{-4}$ MPa^{-2}

plotted by sorting them as ascending with respect to the studied magneto-mechanical cases. Although, there are some variations, the Model I catches the general evolution of the losses under different stress cases. The model is less accurate for the stress states that affect the losses significantly. At these cases Model I usually underestimates the losses. The relative error considering all the cases is calculated by

$$\epsilon = \frac{\|W_{\mathrm{sim}} - W_{\mathrm{tot}}\|}{\|W_{\mathrm{tot}}\|} \tag{7}$$

where W_{sim}, W_{tot} are the simulated and the measured losses, respectively. The errors considering the results from Model I are found to be 13% and 14.2% for magnetization along x and y directions, respectively.

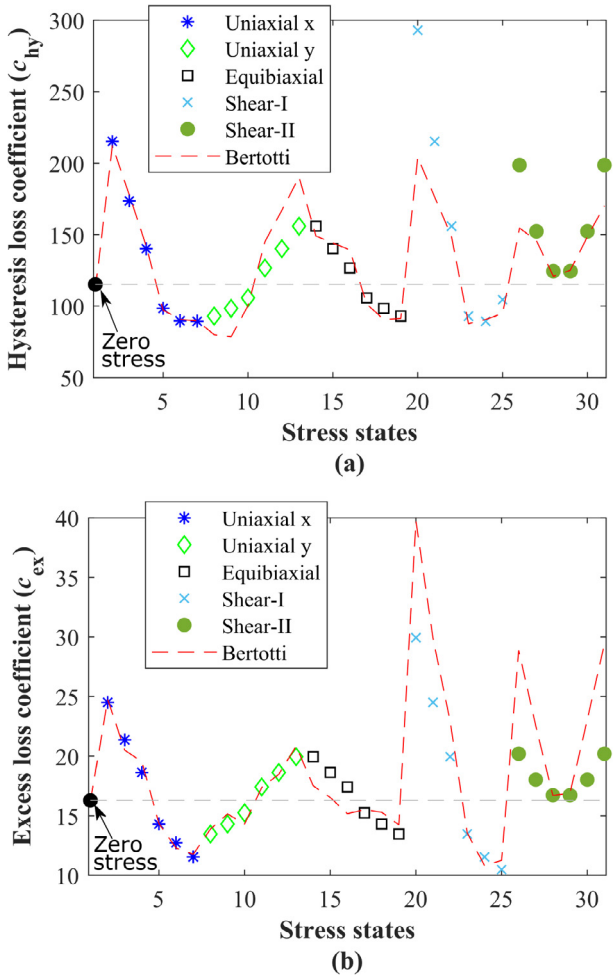

Fig. 14. Modeled loss coefficients by Model II at magnetization along x direction. (a) Hysteresis loss coefficient, (b) Excess loss coefficient. Magnitude of the applied stress varies from −30 MPa to 30 MPa with 10 MPa intervals for each stress case.

3.2.2. Model II

Previously, an energy based invariant model is used to model the stress dependent magnetization and magnetostriction of non-oriented electrical steel sheets [26,35,36]. The model is based on five scalar invariants to describe the magneto-elastic interaction in the material. In this study, in order to model the stress depedency of c_{hy} and c_{ex} a model based on the magneto-elastic invariants given in [26,35,36] is proposed (Model II). These invariants are written as

$$I_5 = \boldsymbol{B}\cdot(\boldsymbol{sB}), \qquad I_6 = \boldsymbol{B}\cdot(\boldsymbol{s}^2\boldsymbol{B}) \tag{8}$$

where $\boldsymbol{B}$ is the direction vector of the flux density and $\boldsymbol{s}$ is the deviatoric part of the applied stress $\boldsymbol{\sigma}$. Then the stress dependent loss coefficients are expressed as a function of I_5 and I_6 as

$$\begin{aligned} c_{\mathrm{hy}}(I_5, I_6) &= c_{0,\mathrm{hy}}(1 + \beta_\mathrm{h} I_5 + \gamma_\mathrm{h} I_6) \\ c_{\mathrm{ex}}(I_5, I_6) &= c_{0,\mathrm{ex}}(1 + \beta_\mathrm{e} I_5 + \gamma_\mathrm{e} I_6) \end{aligned} \tag{9}$$

where $c_{0,\mathrm{hy}}$ and $c_{0,\mathrm{ex}}$ are the Bertotti loss coefficients determined for the stress free case, β_h, γ_h, β_e and γ_e are fitting parameters to be determined. These parameters are obtained by using the measured loss data only for the cases when uniaxial stress is applied parallel to the magnetization direction. Determined parameter values for both the rolling and the transverse directions are given in Table 1.

Using these parameters, the loss coefficients c_{hy} and c_{ex} are modeled under all the studied stress cases where the stress level varies from −30 MPa to 30 MPa with 10 MPa intervals and the results are given in

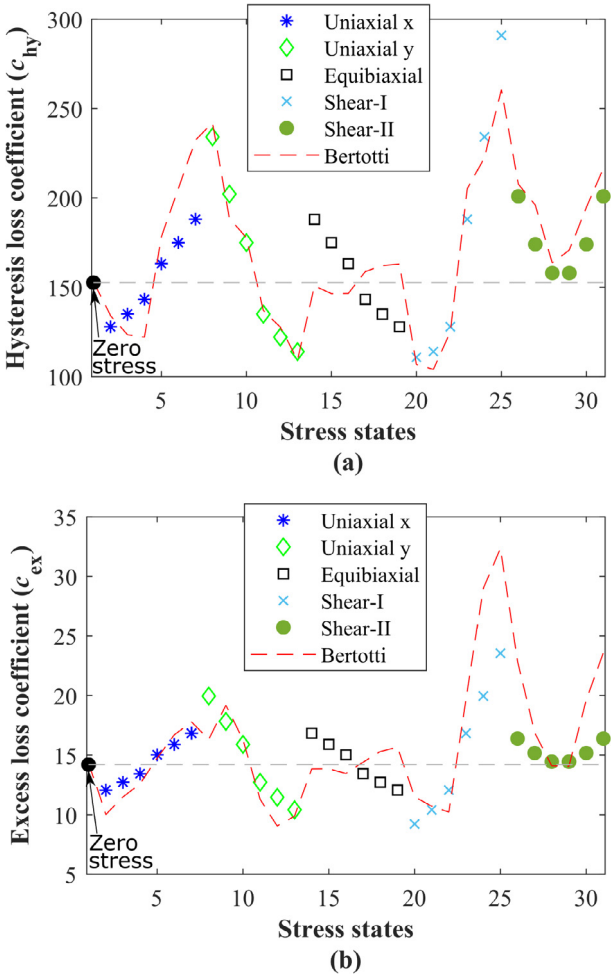

Fig. 15. Modeled loss coefficients by Model II at magnetization along y direction. (a) Hysteresis loss coefficient, (b) Excess loss coefficient. Magnitude of the applied stress varies from −30 MPa to 30 MPa with 10 MPa intervals for each stress case.

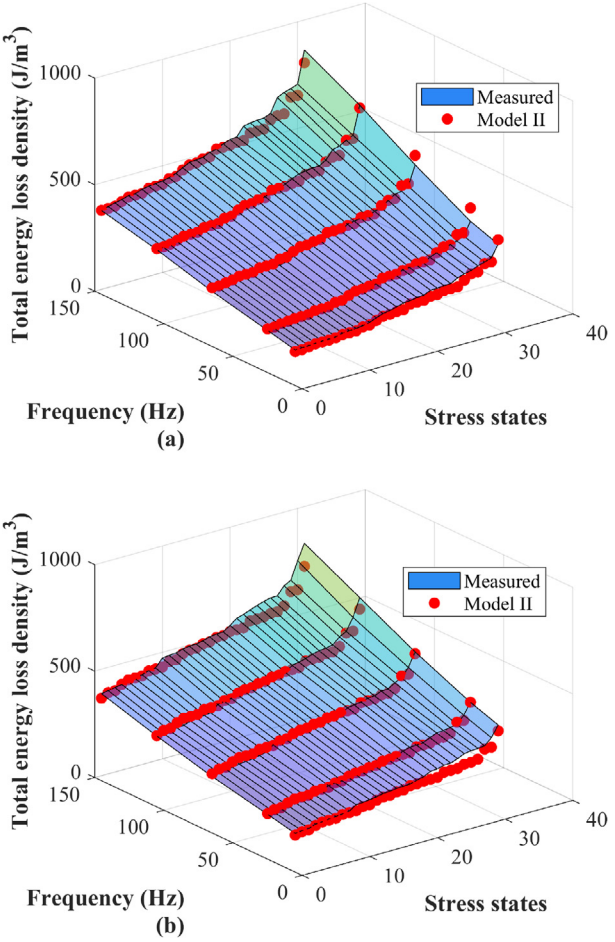

Fig. 16. Total energy loss densities for each stress and magnetization state. Measurements and modeling results from Model II. (a) Magnetization along x direction, (b) Magnetization along y direction. The losses are sorted as ascending.

Figs. 14 and 15 for magnetization along x and y directions, respectively. Considering when the magnetization direction is parallel to x, the model predicts the effect of multi-axial stress on the both loss coefficients with satisfactory accuracy. It is seen that Model II predicts the behavior under shear-II stress configuration as well. The effect of shear-I case $\boldsymbol{\sigma} = [-30 \;\; 30 \;\; 0]^T$ on the c_{hy} is overestimated considerably by Model II which was also the case for Model I. In Fig. 15 modeling results when the magnetization is applied along y direction is shown. Except for the bi-tension case the model catches the evolution of the coefficients under all the stress cases.

It is worth noticing that when the magnetization is along y direction both Model I and Model II predict similar behavior under bi-tension which does not match to the Bertotti loss coefficients that were determined from the measurements. However, the models are successful at predicting the behavior under the same stress state when the magnetization is along x direction. This is because, the application of stress affects the material differently depending on its magnetization condition resulting in different loss evolution. As discussed in Section II A, this is related to the magneto-elastic anisotropy caused by the crystallographic texture variations in the material and neither of the models consider this in their current form. Earlier, in [34], an equivalent stress model was proposed to include the anisotropy for orthotropic materials. Although the model was successful in general, it lacked accuracy for some cases. On the other hand, in order to include the anisotropy for Model II, new invariants should be introduced to the model. This would lead to a higher number of parameters to be identified. The inclusion of magneto-elastic anisotropy is out of scope of this paper. However, a more detailed study on the subject is indeed needed.

The total energy loss densities are modeled by substituting c_{hy} and c_{ex} in (5) with the modeled coefficients from (9) and by dividing the results with the magnetization frequency. The modeled losses by Model II are compared to the measurements in Fig. 16(a) and (b) when the sample is magnetized along x and y directions, respectively. In Fig. 16 the losses are plotted by sorting them as ascending with respect to the studied magneto-mechanical cases. It is observed that Model II is able to predict the stress dependency of the losses for both cases. The errors, calculated by using (7) for when the sample is magnetized along x and y directions are found to be 5.6% and 9.9%. Similarly to Model I, the highest errors for Model II are observed when the effect of stress on the losses are significant.

It can be noticed that Model II can be interpreted as a refined version of an equivalent stress model. In Model I, the equivalent stress is only defined from one magneto-elastic invariant. Model II separates the effect of stress between hysteresis and excess losses, and incorporates two magneto-elastic invariants. This refinement could explain the higher versatility of the second model.

4. Conclusion

Effect of multi-axial stress on the hysteresis and the excess loss components in a grade M400-50A non-oriented electrical steel sheet

was analyzed. For loss separation, magneto-mechanical measurements performed under several multi-axial stress configurations and controlled sinusoidal flux density along rolling and transverse directions with 1 T fixed amplitude at various frequencies were used in Bertotti's statistical loss model. It was observed that under the studied stress states the hysteresis and the excess losses evolve in a similar way and the effect of multi-axial stress on the losses can be much more significant than that of uniaxial stress.

In order to predict the hysteresis and the excess loss evolutions under multi-axial stress, an equivalent stress based model and a magneto-elastic invariant based model are studied. The models are identified by using only uniaxial stress-dependent loss coefficients which were obtained by fitting the Bertotti loss model to the measurements. The accuracy of both models to predict the studied loss components were found to be satisfactory. However, the proposed magneto-elastic invariant based model produced more accurate results. Also under the shear-II stress configuration the invariant based model is able to predict the loss behavior whereas, the studied equivalent stress approach does not model loss evolution under this stress state.

Acknowledgments

The research leading to these results has received funding from the European Research Council under the European Union's Seventh Framework Programme (FP7/2007-2013)/ERC Grant agreement nº339380. P. Rasilo and F. Martin acknowledges the Academy of Finland for financial support under grant nº274593 and nº297345.

References

[1] Y. Kai, Y. Tsuchida, T. Todaka, M. Enokizono, Evaluation of local residual stress distribution of stator core in rotating machine, EEJ Trans. Fundam. Mater. 131 (5) (2011) 389–394.
[2] P. Baudouin, A. Belhadj, F. Breaban, A. Deffontaine, Y. Houbaert, Effects of laser and mechanical cutting modes on the magnetic properties of low and medium si content nonoriented electrical steels, IEEE Trans. Magn. 38 (5) (2002) 3213–3215.
[3] D.J.B. Smith, B.C. Mecrow, G.J. Atkinson, A.G. Jack, A.A.A. Mehna, Shear stress concentrations in permanent magnet rotor sleeves, Proc. Int. Conf. Electr. Mach. ICEM, Rome, Italy, 2010, pp. 1–6.
[4] F. Chai, Y. Li, P. Liang, Y. Pei, Calculation of the maximum mechanical stress on the rotor of interior permanent magnet synchronous motors, IEEE Trans. Ind. Electron. 63 (6) (2016) 3420–3432.
[5] A. Borisavljevic, H. Polinder, J.A. Ferreira, On the speed limits of permanent-magnet machines, IEEE Trans. Ind. Electron. 57 (6) (2010) 220–227.
[6] D. Gerada, A. Mebarki, N. Brown, C.G.K.J. Bradley, Design aspects of high-speed high-power-density laminated-rotor induction machines, IEEE Trans. Ind. Electron. 58 (9) (2011) 4039–4047.
[7] S. Zeze, Y. Kai, T. Todaka, M. Enokizono, Vector magnetic characteristic analysis of a pm motor considering residual stress distribution with complex-approximated material modelling, IEEE Trans. Magn. 48 (11) (2012) 3352–3355.
[8] K. Yamazaki, Y. Kato, Iron loss analysis of interior permanent magnet synchronous motors by considering mechanical stress and deformation of stators and rotors, IEEE Trans. Magn. 50 (2) (2014) 7022504.
[9] K. Yamazaki, W. Fukushima, Loss analysis of induction motors by considering shrink fitting of stator housing, IEEE Trans. Magn. 51 (3) (2015) 8102004.
[10] K. Yamazaki, H. Takeuchi, Impact of mechanical stress on characteristics of interior permanent magnet synchronous motors, IEEE Trans. Ind. Appl. 53 (2) (2017) 963–970.
[11] D. Miyagi, N. Maeda, Y. Ozeki, K. Miki, N. Takashi, Estimation of iron loss in motor core with shrink fitting using fem analysis, IEEE Trans. Magn. 45 (3) (2009) 1704–1707.
[12] L. Bernard, L. Daniel, Effect of stress on magnetic hysteresis losses in a switched reluctance motor: application to stator and rotor shrink fitting, IEEE Trans. Magn. 51 (2015) 7002513.
[13] V. Permiakov, L. Dupre, A. Pulnikov, J. Melkebek, Loss separation and parameters for hysteresis modelling under compressive and tensile stresses, J. Magn. Magn. Mater. 272–276 (2004) e553–e554.
[14] D. Singh, P. Rasilo, F. Martin, A. Belahcen, A. Arkkio, Effect of mechanical stress on excess loss of electrical steel sheets, IEEE Trans. Magn. 51 (11) (2015) 1001204.
[15] J. Karthaus, S. Steentjes, N. Leuning, K. Hameyer, Effect of mechanical stress on different iron loss components up to high frequencies and magnetic flux densities, Int. J. Comput. Math. Electr. Electron. (COMPEL) 36 (2017) 580–592.
[16] K. Ali, K. Atallah, D. Howe, Prediction of mechanical stress effects on the iron loss in electrical machines, J. App. Phys. 81 (1997) 4119–4121.
[17] H. Naumoski, A. Maucher, U. Herr, Investigation of the influence of global stresses and strains on the magnetic properties of electrical steels with varying alloying content and grain size, 5th Int. Elc. Dri. Prod. Conf. (EDPC), 2015, pp. 1–8.
[18] G. Bertotti, General properties of power losses in soft ferromagnetic materials, IEEE Trans. Magn. 24 (1) (1988) 621–630.
[19] Y. Kai, M. Enokizono, Y. Kido, Measurement of vector magnetic properties of nonoriented electrical steel sheet under shear stress, Electr. Eng. Jpn. 191 (2015) 1–7.
[20] Y. Kai, M. Enokizono, Y. Kido, Influence of shear stress on vector magnetic properties on non-oriented electrical steel sheets, Int. J. Appl. Electromagn. Mech. 44 (3–4) (2014) 371–378.
[21] Y. Kai, M. Enokizono, Effect of arbitrary shear stress on vector magnetic properties of non-oriented electrical steel sheets, IEEE Trans. Magn. 53 (11) (2017) 2002304.
[22] M. Rekik, O. Hubert, L. Daniel, Influence of a multiaxial stress on the reversible and irreversible magnetic behaviour of 3% si-fe alloy, Int. J. Appl. Electromagn. Mech. 44 (3–4) (2014) 301–315.
[23] K. Yamazaki, H. Mukaiyama, L. Daniel, Effect of multi-axial mechanical stress on loss characteristics of electrical steel sheets and interior permanent magnet machines, IEEE Trans. Magn. 54 (3) (2017) 1300304.
[24] H. Jordan, Die ferromagnetischen konstanten für schwache wechselfelder, Elektr. Nach. Technol. 1 (1924) 8.
[25] F. Fiorillo, A. Pulnikov, An improved approach to power losses in magnetic laminations under nonsinusoidal induction waveform, IEEE Trans. Magn. 26 (5) (1990) 2904–2910.
[26] U. Aydin, P. Rasilo, D. Singh, A. Lehikoinen, A. Belahcen, A. Arkkio, Coupled magneto-mechanical analysis of iron sheets under biaxial stress, IEEE Trans. Magn. 52 (3) (2016) 2000804.
[27] U. Aydin, F. Martin, P. Rasilo, A. Belahcen, A. Haavisto, D. Singh, L. Daniel, A. Arkkio, Rotational single sheet tester for multiaxial magneto-mechanical effects in steel sheets (Submitted for publication).
[28] K. Matsubara, N. Takahashi, K. Fujiwara, M.N.T. Nakata, H. Aoki, Acceleration technique of waveform control for single sheet tester, IEEE Trans. Magn. 31 (6) (1995) 3400–3402.
[29] D. Singh, Effect of Stress on Magnetic Properties of Electrical Steel Sheet and Core Losses in Electrical Machines (Ph.D. thesis), Aalto University, Espoo/Finland, 2017.
[30] O. Hubert, L. Daniel, R. Billardon, Experimental analysis of the magnetoelastic anisotropy of a non-oriented silicon iron alloy, J. Magn. Magn. Mater. 254–255 (2003) 352–354.
[31] Y. Kai, Y. Tsuchida, T. Todaka, M. Enokizono, Measurement of vector magnetic property under stress along arbitrary direction in non-oriented electrical steel sheet, Przeglad Elektrotechniczny 87 (9b) (2011) 101–105.
[32] L. Daniel, O. Hubert, Equivalent stress criteria for the effect of stress on magnetic behavior, IEEE Trans. Magn. 46 (8) (2010) 3089–3092.
[33] M. Rekik, L. Daniel, O. Hubert, Equivalent stress model for magnetic hysteresis losses under biaxial loading, IEEE Trans. Magn. 50 (4) (2014) 2001604.
[34] O. Hubert, L. Daniel, Energetical and multiscale approaches for the definition of an equivalent stress for magneto-elastic couplings, J. Magn. Magn. Mater. 323 (13) (2011) 1766–1781.
[35] K. Fonteyn, A. Belahcen, R. Kouhia, P. Rasilo, A. Arkkio, Fem for directly coupled magneto-mechanical phenomena in electrical machines, IEEE Trans. Magn. 46 (2010) 2923–2926.
[36] P. Rasilo, D. Singh, U. Aydin, F. Martin, R. Kouhia, A. Belahcen, A. Arkkio, Modeling of hysteresis losses in ferromagnetic laminations under mechanical stress, IEEE Trans. Magn. 52 (2016) 7300204.